

Study of sintered Nd-Fe-B magnet with high performance of H_{cj} (kOe) + $(BH)_{max}$ (MGOe) > 75

Bo-Ping Hu, E. Niu, Yu-Gang Zhao, Guo-An Chen, Zhi-An Chen et al.

Citation: *AIP Advances* **3**, 042136 (2013); doi: 10.1063/1.4803657

View online: <http://dx.doi.org/10.1063/1.4803657>

View Table of Contents: <http://aipadvances.aip.org/resource/1/AAIDBI/v3/i4>

Published by the *AIP Publishing LLC*.

Additional information on AIP Advances

Journal Homepage: <http://aipadvances.aip.org>

Journal Information: <http://aipadvances.aip.org/about/journal>

Top downloads: http://aipadvances.aip.org/features/most_downloaded

Information for Authors: <http://aipadvances.aip.org/authors>

ADVERTISEMENT

Study of sintered Nd-Fe-B magnet with high performance of H_{cj} (kOe) + $(BH)_{max}$ (MGOe) > 75

Bo-Ping Hu,¹ E. Niu,^{1,3,a} Yu-Gang Zhao,^{1,2} Guo-An Chen,^{1,2} Zhi-An Chen,¹

Guo-Shun Jin,¹ Jin Zhang,^{1,2} Xiao-Lei Rao,¹ and Zhen-Xi Wang^{1,3}

¹Beijing Zhong Ke San Huan Research, No.10 Chuangxin Road, Changping District, Beijing 102200, China

²Sanvac (Beijing) Magnetics Co., Ltd, No.23 Chuangxin Road, Changping District, Beijing 102200, China

³State Key Laboratory for Magnetism, Institute of Physics, Chinese Academy of Sciences, P. O. Box 603, Beijing 100190, China

(Received 1 February 2013; accepted 18 April 2013; published online 25 April 2013)

We have developed a Nd-Fe-B sintered magnet of extremely high performance. The intrinsic coercivity H_{cj} is as high as 35.2 kOe (2803kA/m) together with the maximum energy product $(BH)_{max}$ of 40.4 MGOe (321.6kJ/m³). These values result in H_{cj} (kOe) + $(BH)_{max}$ (MGOe) > 75. Between 293 K (20°C) and 473 K (200°C), the temperature coefficients of remanence and intrinsic coercivity are $\alpha_{Br} = -0.122\%/^{\circ}\text{C}$ and $\alpha_{Hcj} = -0.403\%/^{\circ}\text{C}$, respectively. A maximum operating temperature of 503 K (230°C) is obtained when permeance coefficient $P_c = -B/H = 2$. Grain boundary diffusion (GBD) technique on magnet surface has been developed to increase H_{cj} by 3.6 kOe without significantly decrease of B_r and $(BH)_{max}$. The intrinsic coercivity of the GBD treated magnet $H_{cj}(C)$ has a linear relationship with that of the untreated magnet $H_{cj}(B)$ between 200 K and 473 K (in unit of kOe): $H_{cj}(C) = 1.03H_{cj}(B) + 2.38$. The enhancement of H_{cj} by GBD treatment has contributions not only from the improvement of microstructure but also from the increase of H_a in the grain surface layer. It is also found that GBD treatment brings no deterioration in corrosion resistance of untreated magnet. © 2013 Author(s). All article content, except where otherwise noted, is licensed under a Creative Commons Attribution 3.0 Unported License. [<http://dx.doi.org/10.1063/1.4803657>]

I. INTRODUCTION

Invented in 1983,^{1,2} Nd-Fe-B sintered magnets possess outstanding magnetic properties. They are widely applied in various fields such as information technology, home appliance, magnetic resonance image and industry. Sustainable development and green energy create new applications in hybrid or electrical vehicle (HEV or EV), energy-saving appliance, wind mill power generator and so on.^{3,4} Most of these applications require Nd-Fe-B magnets with high maximum energy product $(BH)_{max}$ and high thermal stability which can operate at elevated temperature beyond 200°C.⁵ Excellent thermal stability depends on high Curie temperature (T_C), low temperature coefficient of remanence (α_{Br}), high intrinsic coercivity (H_{cj}) with low temperature coefficient (α_{Hcj}).⁶ Practically high H_{cj} is an essential factor. Unfortunately the increase in H_{cj} always accompanies the decrease in $(BH)_{max}$. Therefore the performance of the magnet should be judged by both H_{cj} and $(BH)_{max}$, rather than by individual H_{cj} or $(BH)_{max}$. For sintered Nd-Fe-B magnets the value of $Q = H_{cj}$ (kOe) + $(BH)_{max}$ (MGOe) may be used as a comprehensive index for judging their performance. The higher the value of Q is, the better performance of the magnet will be. The value Q reflects the technological level of the magnet production. Focusing on the issue of how to produce high

^aElectronic mail: niu@aphy.iphy.ac.cn



performance (big value Q) magnets by improving the thermal stability with little sacrifices in B_r and $(BH)_{\max}$, many efforts have been devoted and much progress has been made in recent years.

Element addition or substitution is a conventional solution. However the merit and demerit are often co-existed for single element. For example, partial substitution of Fe by Co increases T_C and decreases α_{B_r} but reduces H_{c_j} . Thus the thermal stability is not actually improved with overdose of Co.^{3,7-9} On the other hand, partial substitution of Nd by heavy rare earth (HRE) Dy or Tb promotes the magnetocrystalline anisotropy field H_a drastically and greatly increases H_{c_j} .⁹⁻¹¹ However this substitution reduces the saturation magnetization M_s and thus B_r and $(BH)_{\max}$ due to the antiparallel coupling of Fe and Dy/Tb magnetic moments. In addition, element abundance and supply of Dy and Tb is much more limited than Nd.¹² The third solution is to optimize the microstructure of sintered magnets by small amount addition of fusible metals (Al, Cu, Ga) or refractory metals (V, Nb, Mo, *etc.*) to enhance the H_{c_j} . But in most cases, these additives generate phases other than hard magnetic phase $R_2Fe_{14}B$ (R = rare earth) and decrease the B_r and $(BH)_{\max}$.^{10,13-17} Combined addition of different elements, including proper oxygen doping,^{3,6,18,19} is applied to compromise the demerits and achieve high performance.

Different from the element substitution of Dy or Tb, grain boundary diffusion (GBD) treatments have been widely studied recently. In GBD process oxides, fluorides, alloys or even pure metals of Dy or Tb are supplied on the surface of sintered magnets. Dy or Tb atoms diffuse along the grain boundary phase during post-sinter heat treatment at temperature higher than melting point of rare-earth rich (RE-rich) phase but lower than sintering temperature.²⁰⁻²² H_{c_j} can be raised up to 4 ~ 5 kOe without obvious reduction of B_r . Moreover, the composition of Dy or Tb is much lower than those in conventional alloying process, which may reduce magnet cost dramatically. The maximum diffusion depth of GBD-treated magnets is about 6 mm.²³⁻²⁶ However, according to Nakamura *et al.*,²⁶ the H_{c_j} enhancement effect of Dy/Tb GBD-treated magnets depends significantly on the diffusion depth in magnets. The H_{c_j} of the surface part is higher than the H_{c_j} of the inner part due to the content decrease of Dy/Tb from the surface to the center.

Appropriately reducing the grain size of sintered magnet is another way to effectively increase H_{c_j} but make little change of B_r and $(BH)_{\max}$. Sagawa *et al.*^{4,5,27} applied jet mill with Helium gas as medium to bring the average particle size of Nd-Fe-B powder down to ~1 μm . To prevent such fine particles from oxidation, they invented a so-called 'press-less pressing (PLP)' technique to compact fine powder into block in air-tight and oxygen free container. The green parts were sintered in high vacuum. They succeeded in making the Dy or Tb-free Nd-Fe-B magnet of intrinsic coercivity of 20 kOe, which is 9 kOe higher than conventional powder metallurgic process. The $(BH)_{\max}$ is 48 MGOe. Obviously this procedure has great advantage over conventional sintering and GBD process. But it also confronts a lot of difficulties in realizing mass production, such as oxygen contamination and grain size control.

These aforementioned methods make it possible to realize high performance magnet with $H_{c_j}(\text{kOe}) + (BH)_{\max}(\text{MGOe}) \approx 70$.^{19,28} For high temperature applications, it is necessary to keep H_{c_j} higher than 30 kOe and make $(BH)_{\max}$ as large as possible. Manufacture process has to be optimized in every detail to eliminate possible factors of $(BH)_{\max}$ decrease. In this work the production process has been optimized in order to increase the degree of orientation, to decrease the grain size, and to enhance the uniformity of grain size distribution. GBD procedure of fine Dy alloy powder has also been developed. Sintered Nd-Fe-B magnets with $H_{c_j} > 30$ kOe and $H_{c_j}(\text{kOe}) + (BH)_{\max}(\text{MGOe}) > 75$ are achieved and suitable for high-end applications. The intrinsic magnetic properties, extrinsic magnetic properties and microstructure were investigated to unveil their relationship with technical procedure.

II. EXPERIMENTAL

Raw materials was prepared according to a nominal composition of $\text{Pr}_{2.8}\text{Nd}_{8.7}\text{Tb}_{1.9}\text{Dy}_{0.3}(\text{Cu,Al,Ga})_{0.6}\text{Co}_{1.5}\text{Fe}_{\text{bal}}\text{B}_{5.7}$. The addition of Co, Tb and Dy could improve the Curie temperature and magnetocrystalline anisotropy field of the $\text{Nd}_2\text{Fe}_{14}\text{B}$ -structure phase in magnet. The dopants of fusible elements of Al, Cu and Ga could positively influence the wetting behavior of the liquid phase during sintering, then enhance the magnetic decoupling of the

grains²⁹ and the corrosion resistance.³⁰ Alloy flakes were prepared by strip-casting technique. The molten alloy was kept at 1400 °C ~ 1450 °C, and the cooling water at 35 ~ 40 °C. The rotating rate of casting wheel was set to 1.1 m/s and the thickness of the alloy flakes was in an range of 0.3 ~ 0.5 mm. The alloy flakes were crushed by hydrogen decrepitation (HD) process into coarse powder of hundreds microns. With nitrogen gas jet mill, the coarse powder was further milled into fine powder with D_{50} of 6.63 μm . The particle size distribution of fine powder was characterized by a laser particle size analyzer. Under the protection of nitrogen gas, fine powder was aligned in a constant magnetic field of 18.2 kOe (1.45 MA/m) together with alternative field pulses of peak field 40.2 kOe (3.20 MA/m) parallel or antiparallel to the constant field. The powder was pressed to density of 4.2 g/cm³ at a pressure of 120 MPa in the direction perpendicular to magnetic field. The green compacts were then isostatically compacted in oil cylinder under a pressure of 200 MPa. Sintering was undertaken in vacuum at 1080 °C for 3 hours to reach full density and quenching to room temperature by Ar gas blower. Post-sintered magnets were heat-treated in two stages at 900 °C for 2 hours and 500 °C for 3 hours, respectively. This kind of magnet is called “reference magnet” or “Specimen A”.

To improve the performance of the “reference magnet”, the sample preparation routine was optimized in strip casting, jet milling and sintering. Started from the same nominal composition, kept the same temperature range of molten alloy and cooling water as the ‘reference magnet’, alloy strip casting was conducted at rotating rate of 1.5 m/s using a specially designed copper wheel with the diameter 610 mm. The thickness of the alloy flakes was in a range of 0.2 ~ 0.4 mm. The jet milling was also optimized to narrow the particle size distribution with D_{50} of 5.28 μm . To prevent grains from abnormal growing the sintering was at lower temperature of 1020 °C for longer time of 6 hours, compared with the sintering condition of Specimen A. The same two-stage heat-treatment as the Specimen A was taken after sintering. The magnets prepared by this routine are referred as “optimized magnets” or “Specimen B”.

The third way of sample preparation was in the same routine as that for “optimized magnet” except an additional grain boundary diffusion (GBD) treatment. The post-sintered magnets were cut into cylinders of dimensions $\Phi 10.0 \times 10.0 \text{ mm}^3$ or blocks of $50.0 \times 48.0 \times 3.8 \text{ mm}^3$. The cylinders and blocks were coated with Dy alloy powders of several microns in thickness and then were heated at 750 °C ~ 1000 °C for 20 min to 6 h, which was regarded as GBD treatment. Afterwards, the magnets were annealed in the same two-stage condition as Specimen A and Specimen B. The magnets prepared by this routine are referred as “GBD treated magnets” or “Specimen C”.

The chemical composition was determined by inductively coupled plasma (ICP) spectrophotometry. The contents of oxygen, nitrogen and hydrogen were determined by an ONH analyzer (ELTRA ONH2000).

The phase identification and the microstructure were analyzed by X-ray diffraction (XRD) and scanning electron microscope (SEM).

The magnets samples were sliced into cubic of $1.5 \times 1.5 \times 1.5 \text{ mm}^3$ for measuring magnetization. A Lakeshore 7410 vibrating sample magnetometer (VSM) was used to measure the temperature dependence of magnetization (M) in an applied field of 300 Gs (23.9 kA/m) to determine the Curie temperature T_C . The magnetization curves were measured by a superconducting quantum interference device (SQUID) VSM with the maximum field of 70 kOe (5.57 MA/m).

Because of the pole-piece saturation effect in close-loop measurement, the room temperature demagnetization curves were measured by a pulse field magnetometer PFM12.cn with the peak field up to 100 kOe (7.96 MA/m). The demagnetization curves of specimens from 120 °C to 200 °C were measured by a Magnet-Physik permagraph C-300. Samples for close-loop measurements were $\Phi 10.0 \times 10.0 \text{ mm}^3$ cylinders. The temperature-dependent irreversible flux losses were deduced from the magnetic flux differences of the magnets at 20 °C and a fixed temperature (up to 250 °C) for 2 hours. The magnetic flux was measured by Lakeshore Helmholtz coil and fluxmeter. The permeance coefficients ($P_c = -B/H$) of samples were chosen as 0.5, 1.0 and 2.0, respectively, by cutting samples from blocks with the same thickness of 3.8 mm and different diameters. The maximum operating temperature for a magnet with a certain P_c value is defined by the temperature point at which the absolute value of irreversible flux loss is 5%.

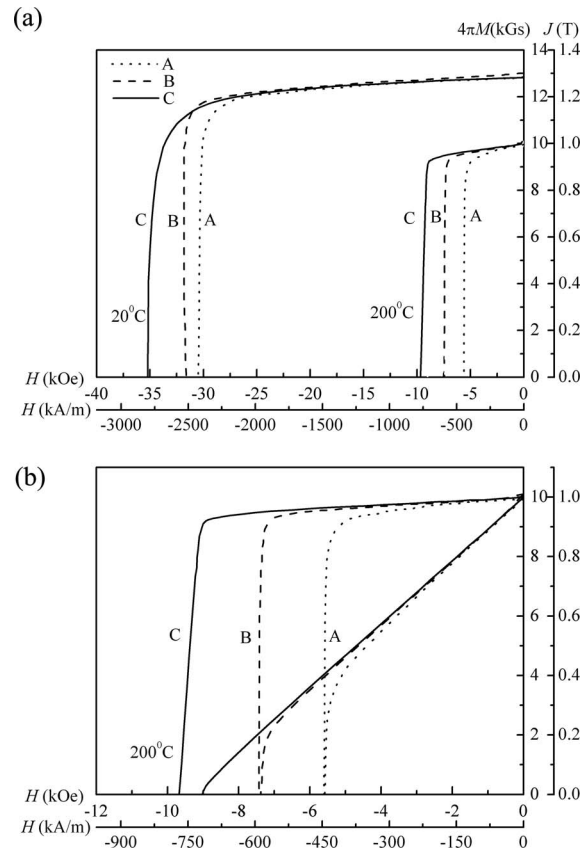


FIG. 1. Demagnetization curves of (a) $4\pi M-H$ at 20°C and 200°C, (b) $4\pi M-H$ and $B-H$ at 200°C of reference magnet (Specimen A, the dot line), optimized magnet (Specimen B, the dash line) and GBD treated magnets (Specimen C, the continuous line) at 20°C and 200°C. (Close-loop measurement and sample dimension: $\Phi 10.0 \times 10.0 \text{ mm}^3$)

The corrosion resistance is characterized by the weight loss measured after the accelerated aging test. A pressure cook test (PCT) chamber was employed under the test condition of 120°C and 100%RH (relative humidity) with condensation of water vapor (according to JEDEC standard: JESD22-A102D, Accelerated Moisture Resistance-Unbiased Autoclave).

III. RESULTS AND DISCUSSION

A. Extrinsic magnetic properties and thermal stability of magnets

Fig. 1(a) shows the $4\pi M-H$ demagnetization curves of reference magnet (Specimen A), optimized magnet (Specimen B) and GBD treated magnet (Specimen C) at temperatures of 20°C and 200°C, respectively. Fig. 1(b) shows $B-H$ curves together with $4\pi M-H$ curves at 200°C. The extrinsic magnetic parameters between 20°C and 200°C are summarized in Table I and Fig. 2. Comparing to Specimen A, Specimen B with optimized routine has its $(BH)_{\max}$ increased by 0.6 MGOe and H_{c_j} by 1.2 kOe at 20°C. According to a high magnetic performance description, by adding data of H_{c_j} and $(BH)_{\max}$ in Gaussian unit we can get $H_{c_j}(\text{kOe}) + (BH)_{\max}(\text{MGOe}) = 72.5$. The Specimen A only has this value of 70.7. Obviously the optimized routine significantly improves the performance of the magnet. In addition, Specimen C (GBD treated magnet) has B_r of 12.8 kGs (1.28 T), H_{c_j} of 35.2 kOe (2803 kA/m) and $(BH)_{\max}$ of 40.4 MGOe (321.6 kJ/m³). The B_r decreases slightly compare to Specimen B. The H_{c_j} increases drastically with 3.6 kOe by GBD treatment which brings the value of $H_{c_j}(\text{kOe}) + (BH)_{\max}(\text{MGOe})$ up to 75.6. At 200°C the $B-H$ curve of GBD treated magnet has no obvious knee point. This implies that the GBD treated magnets can be applied at temperature

TABLE I. The magnetic properties of reference magnet (Specimen A), optimized magnet (Specimen B) and GBD treated magnet (Specimen C) at different temperatures. (Close-loop measurement and sample dimension: Φ 10.0 \times 10.0 mm³)

Parameters T ($^{\circ}\text{C}$)	B_r (kGs)			H_{cj} (kOe)			$(BH)_{max}$ (MGOe)			$H_{cj}(\text{kOe}) +$ $(BH)_{max}(\text{MGOe})$		
	A	B	C	A	B	C	A	B	C	A	B	C
20	12.8	13.0	12.8	30.4	31.6	35.2	40.3	40.9	40.4	70.7	72.5	75.6
100	11.9	12.0	11.9	17.8	19.4	— ^a	33.4	33.9	33.6	51.2	53.3	— ^a
120	11.6	11.7	11.6	15.6	16.7	19.7	31.5	32.0	31.8	47.1	48.7	51.5
140	11.1	11.3	11.1	13.0	14.2	17.3	29.0	29.6	29.2	42.0	43.8	46.5
160	10.8	11.0	10.8	10.3	11.9	14.6	27.5	28.0	27.6	37.8	39.9	42.2
180	10.2	10.4	10.2	7.81	9.55	12.1	24.5	25.1	24.8	32.3	34.7	36.9
200	9.96	10.1	10.0	5.59	7.43	9.67	22.8	23.2	23.0	28.4	30.6	32.7

^aThe H_{cj} value of GBD treated magnet at the temperature of 100 $^{\circ}\text{C}$ is beyond the measuring range of the Magnet-Physik permagraph C-300.

up to 200 $^{\circ}\text{C}$. Contrastively, both Specimen A and B have knee points on their B - H curves at this temperature (see Fig. 1(b)).

From Table I and Fig. 2 it can be recognized that all the extrinsic magnetic parameters decrease with the increase of temperature. The difference of B_r between Specimen A and Specimen B keeps at 0.1 \sim 0.2 kGs (see Fig. 2(a)). The $(BH)_{max}$ of Specimen B are 0.4 \sim 0.6 MGOe higher than Specimen A (Fig. 2(c)). The B_r of Specimen C is nearly the same as Specimen A in the whole temperature range. Because of the improvement of squareness in demagnetization curve, the $(BH)_{max}$ of Specimen C is slightly higher than Specimen A. Obvious change occurs on the intrinsic coercivity H_{cj} . With optimized routine H_{cj} of Specimen B enhance by 1.1 \sim 1.8 kOe compare to Specimen A. The GBD treatment adds another 2.2 \sim 3.6 kOe to H_{cj} (see Fig. 2(b)). Subsequently the optimized routine has positive effect to increase the sum of H_{cj} (kOe) and $(BH)_{max}$ (MGOe) by 1.6 \sim 2.4. Meanwhile the GBD treatment improves the sum of Specimen C by 2.1 \sim 3.1 within the whole temperature range compare to Specimen B. The temperature coefficient of B_r is defined as $\alpha_{Br} = (B_r(T) - B_r(T_0))/(B_r(T_0)(T - T_0))$. The corresponding temperature coefficient of H_{cj} is $\alpha_{Hcj} = (H_{cj}(T) - H_{cj}(T_0))/(H_{cj}(T_0)(T - T_0))$. Between 20 $^{\circ}\text{C}$ and 200 $^{\circ}\text{C}$ the temperature coefficients of B_r and H_{cj} are $\alpha_{Br}(B) = -0.124 \text{ \%}/^{\circ}\text{C}$ and $\alpha_{Hcj}(B) = -0.425 \text{ \%}/^{\circ}\text{C}$ for optimized magnets. These values become $\alpha_{Br}(C) = -0.122 \text{ \%}/^{\circ}\text{C}$ and $\alpha_{Hcj}(C) = -0.403 \text{ \%}/^{\circ}\text{C}$ for GBD treated magnets. While α_{Br} is nearly the same value, α_{Hcj} is reduced by about 5%. This indicates that the GBD treatment enhances the intrinsic coercivity efficiently at all measured temperatures so that temperature coefficients of H_{cj} have improved. The GBD treatment has little effect on the temperature coefficient of remanence.

Fig. 3 and Table II illustrate the irreversible flux loss of the magnets of Specimen B and C for different permeance coefficients $P_c = -B/H = 0.5, 1.0, 2.0$ after exposure at the temperatures of 26 $^{\circ}\text{C}$, 120 $^{\circ}\text{C}$, 150 $^{\circ}\text{C}$, 180 $^{\circ}\text{C}$, 200 $^{\circ}\text{C}$, 220 $^{\circ}\text{C}$, 230 $^{\circ}\text{C}$, 240 $^{\circ}\text{C}$ and 250 $^{\circ}\text{C}$ for 2 hours, respectively. The irreversible flux loss³¹ is defined by $(\Phi(T) - \Phi(20^{\circ}\text{C}))/\Phi(20^{\circ}\text{C})$, where the magnetic flux $\Phi(T)$ was measured at room temperature after the magnet exposed at high temperature T for 2 hours. It can be seen that all the absolute values of irreversible loss are less than 3% below 200 $^{\circ}\text{C}$, no matter what the treatment and P_c are. Therefore even the samples of optimized magnet with P_c no less than 0.5 can be stably used at 200 $^{\circ}\text{C}$. At higher temperature, the absolute values of irreversible losses increase drastically with decrease of P_c . The samples of optimized magnet show larger loss comparing to the samples of GBD treated magnet of the same P_c at the same temperature. The maximum working temperature for a magnet with a certain P_c value is usually defined as the temperature at which the absolute value of irreversible loss is 5%. It can be recognized from Fig. 3 that the maximum working temperatures of Specimen C are 5 \sim 10 $^{\circ}\text{C}$ higher than Specimen B. In other words GBD treated magnets have better thermal stability than optimized magnets. The maximum working temperature of GBD treated magnet with $P_c = 2.0$ is higher than 230 $^{\circ}\text{C}$, which means that GBD magnets may meet the demands of many applications such as hybrid or electrical vehicle (HEV or EV), energy-saving appliance, wind mill power generator and so on.

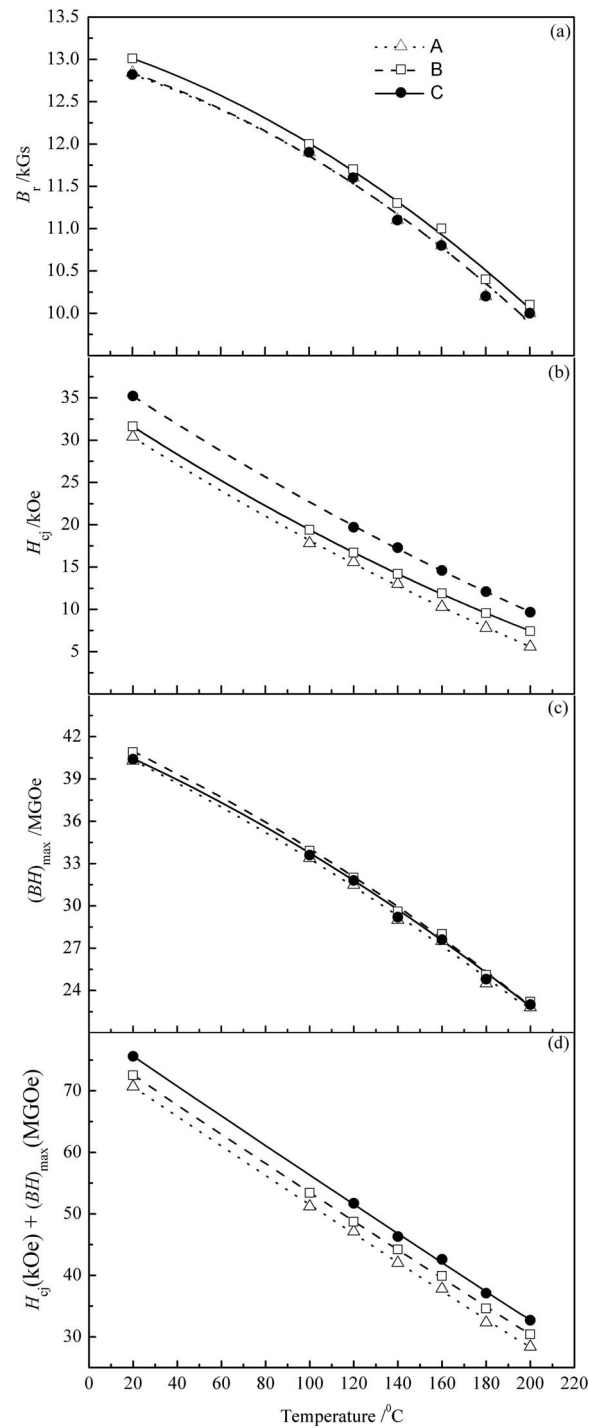


FIG. 2. The temperature dependence of (a) remanence B_r , (b) intrinsic coercivity H_{cj} , (c) the maximum energy product $(BH)_{max}$ and (d) H_{cj} (kOe) + $(BH)_{max}$ (MGOe) of reference magnet (Specimen A, the dot line with triangle symbol), optimized magnet (Specimen B, the dash line with square symbol) and GBD treated magnet (Specimen C, the continuous line with circular symbol).

TABLE II. Irreversible flux losses of optimized magnet (Specimen B1, B2, B3) and GBD treated magnet (Specimen C1, C2, C3) at different working points ($P_c = -B/H = 0.5, 1.0, 2.0$) and temperatures. The uncertainty for the measurement is about 0.6%.

Temperature °C	Irreversible flux losses of Specimen B (optimized magnet), %			Irreversible flux losses of Specimen C (GBD treated magnet), %		
	B1	B2	B3	C1	C2	C3
	$P_c = 0.5$	$P_c = 1.0$	$P_c = 2.0$	$P_c = 0.5$	$P_c = 1.0$	$P_c = 2.0$
26	0.0	0.0	0.0	0.0	0.0	0.0
85	-0.3	-0.1	-0.1	0.1	0.2	-0.2
100	-0.4	-0.3	-0.3	0.0	0.1	-0.4
120	0.2	-0.2	-0.4	0.0	0.1	-0.4
150	-0.5	-0.3	-0.7	-0.1	0.0	-0.5
180	-0.9	-0.7	-0.8	-0.4	-0.3	-0.8
200	-1.9	-1.2	-1.1	-0.8	-0.6	-1.2
220	-18.7	-4.2	-2.2	-9.0	-1.6	-2.0
230	-30.8	-12.5	-4.5	-20.4	-5.0	-3.3
240	-42.4	-24.6	-7.8	-32.1	-13.7	-5.5
250	-55.3	-39.9	-15.9	-46.5	-28.7	-10.1

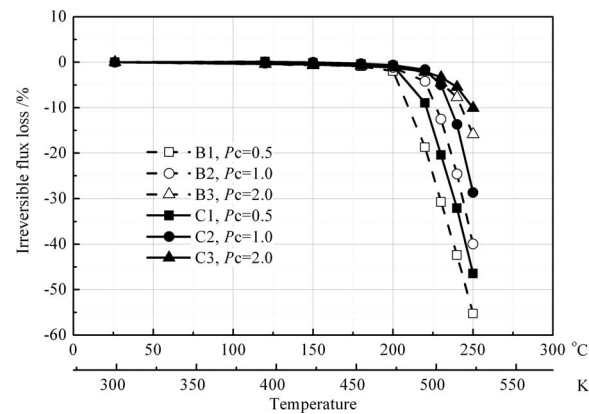


FIG. 3. Irreversible flux losses of optimized magnet (Specimen B1, B2, B3, the dash lines with hollow symbols) and GBD treated magnet (Specimen C1, C2, C3, the continuous lines with solid symbols) at different working points ($P_c = -B/H = 0.5, 1.0, 2.0$) as a function of temperature.

B. Microstructure of magnets and related alloys

Large field images observed by optical microscope are shown in Fig. 4 for reference magnet (Fig. 4(a)), optimized magnet (Fig. 4(b)) and GBD treated magnet (Fig. 4(c)). The images were taken on the surface perpendicular to magnetic orientation direction. From Fig. 4(b) and 4(c) it can be estimated that the grain sizes of matrix phase are from 2 to 15 μm with an average of 7 μm . There is no abnormally growing large grain and even no two grains join together. The net-like black lines of etched RE-rich phase obviously indicate that fine matrix grains are well separated from each other. This metallurgic structure is essential for Nd-Fe-B magnets to achieve high coercivity. For comparison, the image of reference magnet (Fig. 4(a)) shows an average grain size of 10 μm . The notable difference of Fig. 4(a) to Fig. 4(b) and 4(c) is the existence of 20 μm large grains and sub-micron fine grains. Abnormally grown large grains in reference magnet are responsible for the relatively low H_{cj} . In addition, the very fine grains will decrease both B_r and H_{cj} because of their strong tendency of oxidation and misalignment.

Several efforts have been made in optimized manufacturing routine to result in such differences. The technique of strip casting is helpful for the starting R-Fe-B alloy to uniformly disperse RE-rich phase and depress the growth of α -Fe phase.³² With optimized structure of tundish the temperature

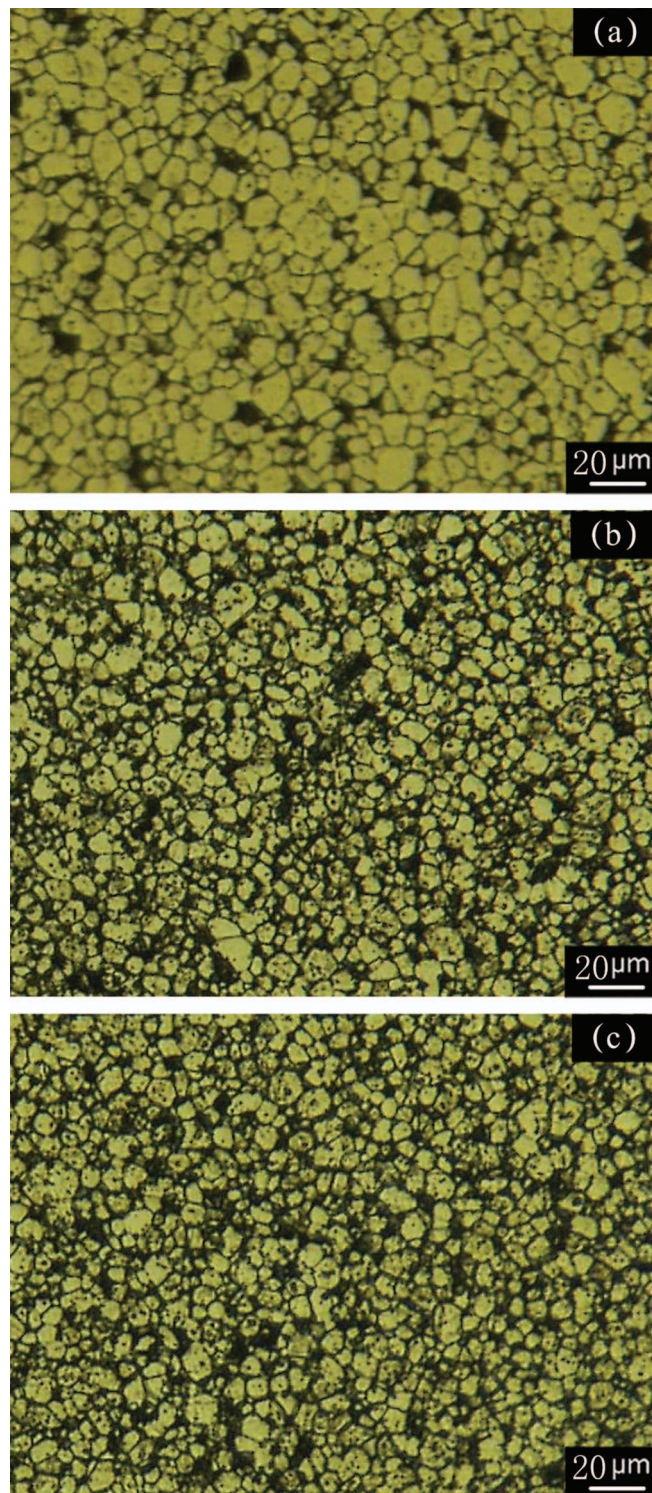


FIG. 4. Optical microscopic images with the normal direction parallel to magnetic orientation direction of (a) reference magnet, (b) optimized magnet, (c) GBD treated magnet.

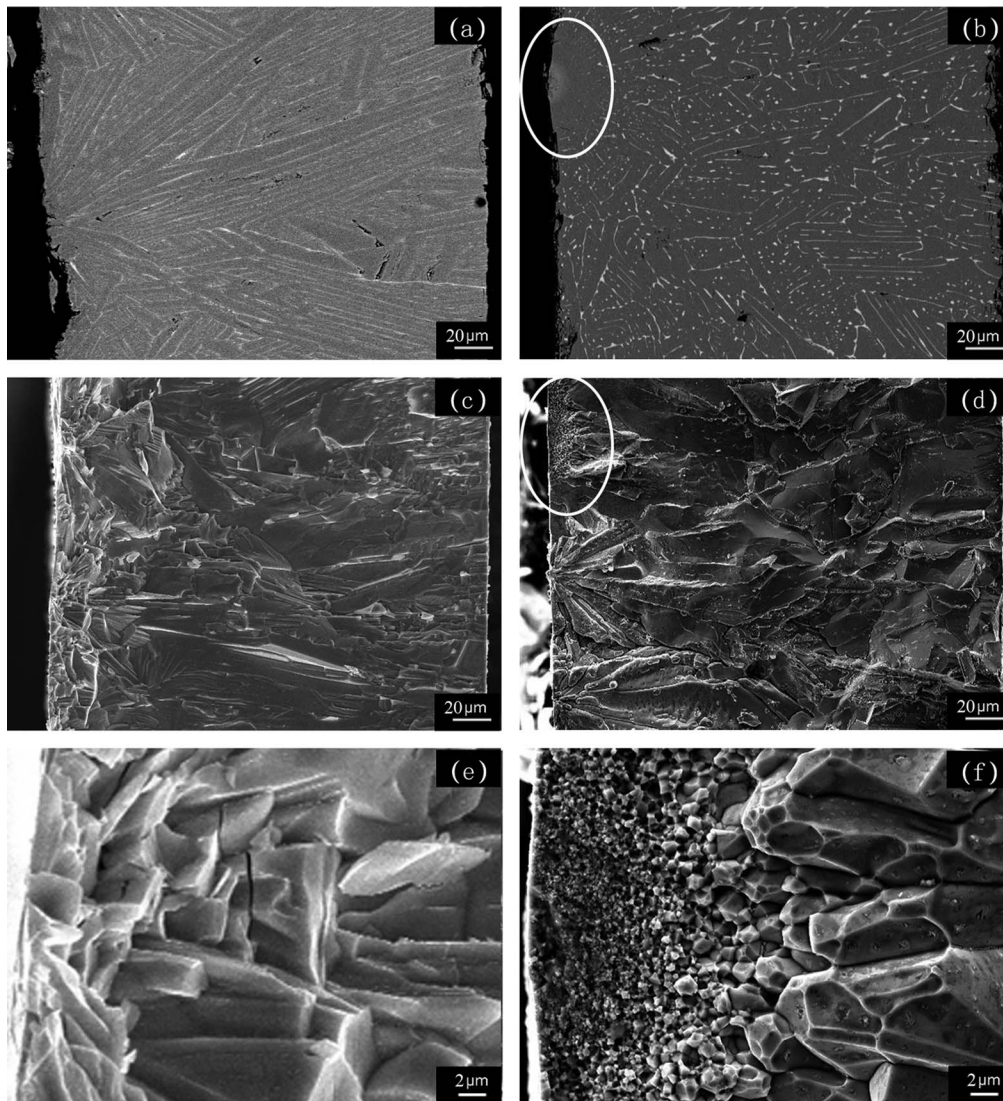


FIG. 5. The microstructure comparison of optimized strip-casting (SC) alloy (a), (c), (e) and the conventional SC alloy (b), (d), (f). The left side of each photo is the wheel-contact surface while the right side is the free surface. (a) and (b) are the BSE (Back Scattered Electron) images of polished samples. (c), (d), (e), (f) are the second electron images of samples' fracture section. (e) and (f) are the detail views of the wheel-contact surface.

in melt pool keeps homogeneous during alloy cast.³³ Together with optimized wheel spinning rate an ideal microstructure of strip-casting alloy have been achieved. Fig. 5(a) and Fig. 5(b) show the SEM back scattered electron images (BSE) of strip-casting alloy prepared by optimized process and conventional method, respectively. It can be seen that the thicknesses of the strip-casting alloy are 0.2 ~ 0.4 mm. The columnar grains (the dark areas) are about 3 ~ 5 μm in width and well separated by the uniformly distributed RE-rich phase (the white lines). Across the thickness direction from the wheel-contact surface to the free surface, the grains of optimized process are uniformly distributed (Fig. 5(c) and Fig. 5(e)). Different from the optimized strip-casting process, in conventional strip-casting alloy there are ultra-fine grain zones on the wheel-contact surface (areas with white elliptical mark in Fig. 5(b) and Fig. 5(d)). Further enlarged image (Fig. 5(f)) shows that the ultra-fine zone contains submicron isometric grains of matrix phase. During jet milling some of these submicron isometric crystals may keep in multi-crystalline status which is proven to be harmful to powder orientation.³⁴ The remanence perpendicular to the orientation direction B_r^\perp was measured on

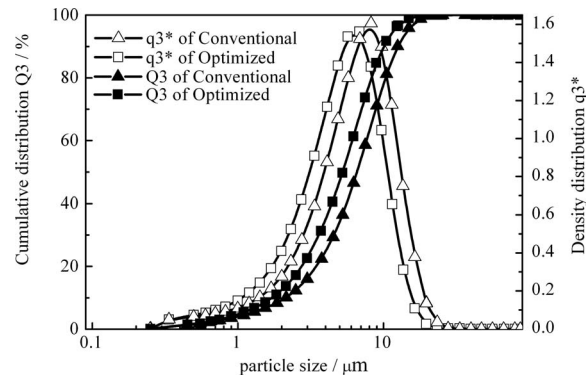


FIG. 6. Particle size distribution of conventional crushing process and optimized process.

Specimen A and B magnets. They are 0.89 kGs and 0.80 kGs, respectively. Dividing B_r^\perp by B_r in Table I one can get the ratio of B_r^\perp / B_r as 7.0% for reference magnet and 6.2% for optimized magnet. The degree of orientation in reference magnet is slightly distorted. Other submicron isometric crystals may be crushed into sub-micron single-crystalline particles. Then they are eliminated into dust collector. The total rare earth composition will decrease and the liquid-phase sintering process will be negatively affected.³⁴ The ICP analysis revealed the composition results. The total rare earth compositions are 30.95 wt.% for optimized magnet and 30.60 wt.% for reference magnet, even though they started from the same nominal composition. Therefore the metallurgical structure of strip-casting alloy plays a critical role in optimizing the magnetic properties.

Narrow distribution of fine grains in optimized magnet is also ensured by optimized crushing process. Fig. 6 compares the particle size distribution of optimized and conventional crushing process. The optimized crushing process leads to a very narrow particle size distribution. The measurement of particle size distribution reveals that the D_{50} is 5.28 μm for optimized crushing process, while 6.63 μm for the conventional process. The very large particles may lead to abnormal grain growth during sintering. The over-grown grains will damage the coercivity and the squareness of demagnetization curve. It is worth noting that the D_{50} is comparable to the width of the columnar grains in alloy strips. Together with low temperature and long time sintering, the optimized magnet with fine grains is realized to ensure high coercivity.

Normally a two-step annealing at temperature of 900 °C for 2 hours and 500 °C for 3 hours was applied to the post-sintered magnets. Fig. 7(a) and Fig. 7(b) compare the microstructures of magnets before and after annealing, respectively. In as-sintered magnet (Fig. 7(a)) patches of RE-rich phases can be seen to concentrate in triple-junctions and corners of main phase grains. It is hard to recognize any thin RE-rich phase penetrating into two-grain boundary. However, in two-stage annealed magnet (Fig. 7(b)) there are continuous thin RE-rich phases along the grain boundaries with scattered RE-rich concentrated junctions. After GBD treatment, more distinct, continuous and thinner RE-rich phase between the grain boundaries can be seen in the magnet (Fig. 7(c)). Apparently, two-stage annealing and the GBD treatment uniformly disperse the RE-rich phases into grain boundaries to completely isolate the matrix phase grains.

During manufacturing process O, H, or N contamination is inevitable and sensitive to magnetic properties. Oxygen content in strip-casting alloy flake was determined by ONH analyzer as 100 ppm. In optimized magnet and GBD treated magnet the oxygen contents increased to be 1000 ppm. The hydrogen content is about 1.3 ppm and the nitrogen content is less than 110 ppm. The X-ray diffraction pattern of grinded magnet shows a $\text{Nd}_2\text{Fe}_{14}\text{B}$ -structure phase together with a tiny hint of R_2O_3 phase. Supposing all oxygen atoms exist in form of R_2O_3 , it can be deduced that there is about 0.71 wt.% of R_2O_3 in magnets. Over dosage of oxygen contamination is considered to be harmful for forming smooth thin RE-rich phase, thus decreases the coercivity dramatically.³⁵ Fig. 8(a) shows the metallographic image of optimized magnet on the surface perpendicular to magnetic orientation direction. The image is binarized to whiten the $\text{Nd}_2\text{Fe}_{14}\text{B}$ -structure main phase and leave the grain boundary as black (Fig. 8(b)). Based on the area method of the Quantitative

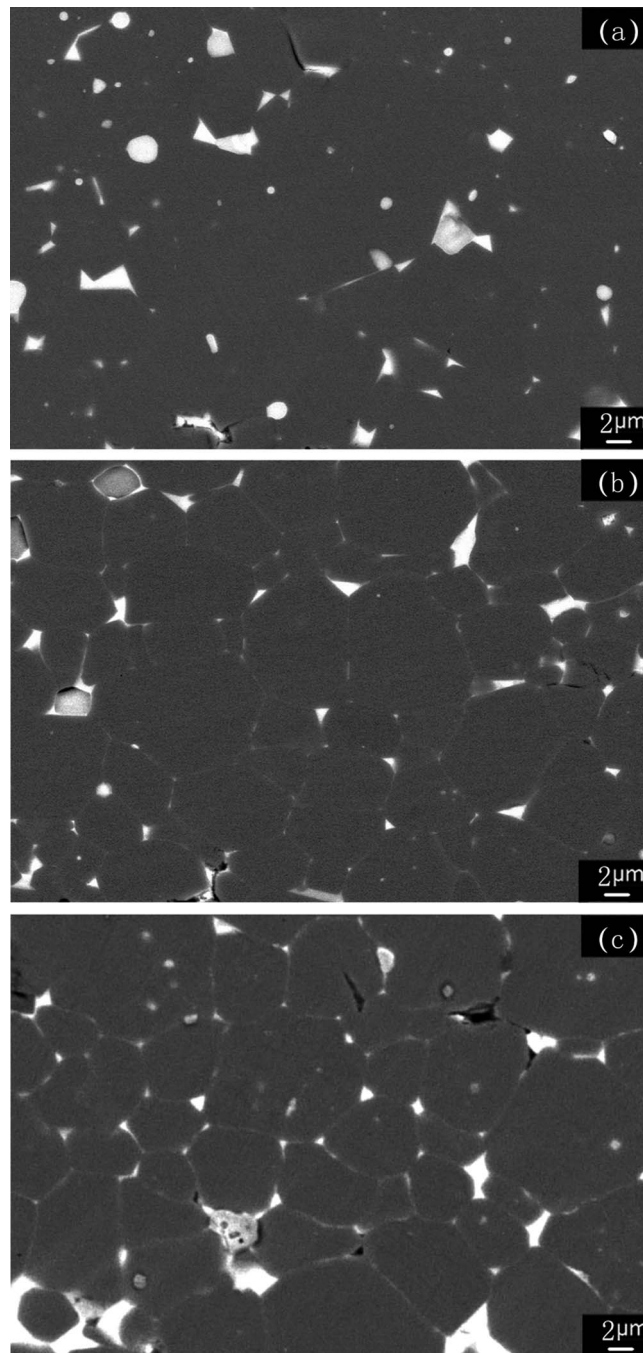


FIG. 7. BSE images of magnets with the normal direction parallel to magnetic orientation direction, (a) optimized magnet before annealing, (b) optimized magnet after annealing, (c) GBD treated magnet.

Metallographic Analysis (QMA) system, together with the software Image-Pro Plus (IPP), the area ratio of the main phase are estimated. Three different zones of $0.6 \times 0.5 \text{ mm}^2$ have been selected and analyzed under the magnification of $500\times$. The area ratios of main phase are 94.6%, 94.9% and 94.6%, respectively. The average value is 94.7%. With this area ratio the main phase grains are well separated by black net lines. The RE-rich phase is sufficient to form nonmagnetic intergranular phase to completely isolate matrix phase. If there were too much oxygen, the R-rich phase would be insufficient. Neighbor grains of main phase have tendency to join each other directly. This phenomenon is equivalent to abnormal grown large grains in magnet which decreases intrinsic coercivity.

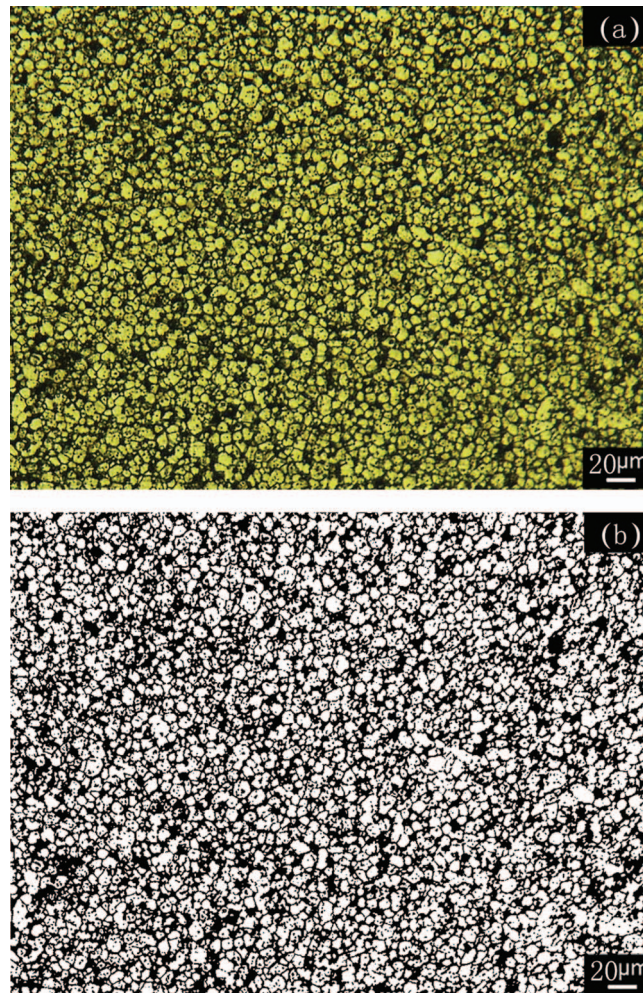


FIG. 8. The metallography images of the cross-section with the normal direction parallel to magnetic orientation direction before binarization (a) and after binarization (b).

C. Intrinsic magnetic properties and intrinsic coercivity before and after GBD treatment

The intrinsic magnetic properties of the rare-earth transition-metal intermetallic compounds $(R_1, R_2, \dots, R_i, \dots, R_n)_2(T_1, T_2, \dots, T_j, \dots, T_m)_{14}B$ can be predicted by taking the corresponding values of individual isostructural $R_2T_{14}B$ compound. From ICP analysis the strip-casting alloy flake has a composition of $Pr_{2.79}Nd_{8.68}Tb_{1.90}Dy_{0.28}(Cu, Al, Ga)_{0.58}Co_{1.50}Fe_{78.51}B_{5.76}$. If considering all Fe and Co atoms form $Nd_2Fe_{14}B$ -structure phase and Cu, Al and Ga enter into R-rich phase, one may deduce the formula of the $R_2T_{14}B$ phase as $Pr_{0.41}Nd_{1.27}Tb_{0.28}Dy_{0.04}Co_{0.26}Fe_{13.74}B$. The remaining rare earth and oxygen exist as R-rich phase or R-oxide. Taking the weighted average over corresponding values of individual intermetallic compounds $R_2Fe_{14}B$ and $R_2Co_{14}B$ ($R = Pr, Nd, Tb, Dy$), the saturation polarization $4\pi M_s = 14.4$ kGs can be predicted. To make a more accurate estimation of $4\pi M_s$, the volume ratio of $Nd_2Fe_{14}B$ -structure main phase has to be considered. As discussed above, by taking the volume fraction of 94.7% for the main phase, the saturation polarization $4\pi M_s$ will be 13.6 kGs. Together with room temperature magnetocrystalline anisotropy field H_a of $Nd_2Fe_{14}B$ as 76 kOe, $Tb_2Fe_{14}B$ as 220 kOe and $Dy_2Fe_{14}B$ as 150 kOe,¹⁰ the magnetocrystalline anisotropy field $H_a = 99.7$ kOe is expected. In $R_2(Fe, Co)_{14}B$ intermetallic compounds, the Curie temperature T_C is mainly determined by exchange interaction of Fe-Co sub-lattice and partially affected by R-(Fe, Co) and R-R interactions. According to the composition the relative percentage of Co substitution

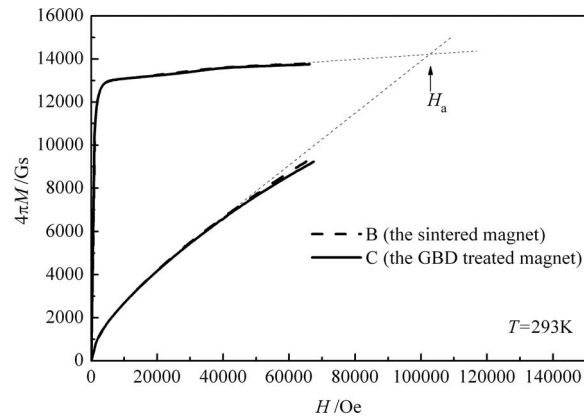


FIG. 9. Initial magnetization curves of directions along the easy magnetization direction and the hard magnetization direction for the optimized magnet and the GBD treated magnet.

of Fe is 1.37 at.%. Based on the T_C - x curve of Curie temperature T_C against Co content x in $\text{Nd}_2(\text{Fe}_{1-x}\text{Co}_x)_{14}\text{B}$,^{8,16,36} the T_C of the strip-casting alloy should be 324 °C.

For comparison of prediction and measurement, the density of magnet has to be obtained first. From X-ray diffraction the lattice parameters of $\text{Nd}_2\text{Fe}_{14}\text{B}$ -structure main phase for all specimens have the same values of $a = 0.879$ nm and $c = 1.218$ nm. It indicates that GBD treatment does not affect main phase. If taking the lattice parameters of individual $\text{R}_2(\text{Fe},\text{Co})_{14}\text{B}$ intermetallic compound ($\text{R} = \text{Pr}, \text{Nd}, \text{Tb}, \text{Dy}$) in accordance with the composition of $\text{Pr}_{0.41}\text{Nd}_{1.27}\text{Tb}_{0.28}\text{Dy}_{0.04}\text{Co}_{0.26}\text{Fe}_{13.74}\text{B}$, the lattice parameters of $a = 0.879$ nm and $c = 1.216$ nm may be obtained, which are well agreed with the experimental results. From the room temperature measurement, we obtained the density of optimized magnets and GBD treated magnets. They have the same value of $\rho_m^{\text{exp}} = 7.621 \text{ g/cm}^3$.

The magnetization curves of an optimized magnet (Specimen B) and a GBD treated magnet (Specimen C) were measured in the applied fields up to 70 kOe along the easy magnetization direction (parallel to the magnetic orientation direction) and the hard direction (perpendicular to the magnetic orientation direction). The magnets were cubic with side length of 1.5 mm. And one edge was chosen as parallel to the orientation direction. Fig. 9 gives the typical magnetization curves at temperature of 20 °C. The open circuit measurements were corrected by a demagnetization factor $N = 0.26$.³⁷ The saturation polarization $4\pi M_s$ is deduced from the magnetization curve along easy direction with density of $\rho_m^{\text{exp}} = 7.621 \text{ g/cm}^3$. The $4\pi M_s$ is 13.3 kGs for the optimized magnet and 13.2 kGs for the GBD treated magnet. These values are slightly smaller than that of the strip-casting alloy flake and the predicted value.

The magnetocrystalline anisotropy field H_a is estimated from the cross point of extension lines of the $4\pi M$ - H curves along easy and hard directions (Fig. 9). In both directions, the polarization $4\pi M$ of the GBD treated magnet is slightly smaller than that of the optimized magnet. The magnetocrystalline anisotropy field H_a has almost the same value of 104 kOe for both magnets. This value is higher than the predicted value of 99.7 kOe from composition. The misalignment of main phase grains of the magnet may affect the extrapolation of magnetization curve along hard magnetization direction.

The measured value of Curie temperature T_C is nearly the same as 334 °C for strip-casting alloy, the optimized magnet and the GBD treated magnet. Comparing to $T_C = 315$ °C of the pure $\text{Nd}_2\text{Fe}_{14}\text{B}$, the T_C increases by 19 °C. This contribution is mainly from Co substitution since the T_C of $\text{Nd}_2\text{Co}_{14}\text{B}$ is as high as 727 °C. Different from the prediction of 324 °C, another 10 °C increase in T_C comes from rare earth substitution. Although the substitution of Nd by Pr slightly decreases T_C , the overall rare earth effect is positive. Co substitution has another positive effect to increase magnetization of $\text{Nd}_2\text{Fe}_{14}\text{B}$ if the relative composition of Co to Fe is less than 20 at.%. However Co substitution is accompanied with the regressing of anisotropy.^{38,39} Therefore the Co addition is limited.

The measured parameters of intrinsic magnetic property have a good match with the prediction based on the $\text{Pr}_{0.41}\text{Nd}_{1.27}\text{Tb}_{0.28}\text{Dy}_{0.04}\text{Co}_{0.26}\text{Fe}_{13.74}\text{B}$ compound. And more importantly it indicates

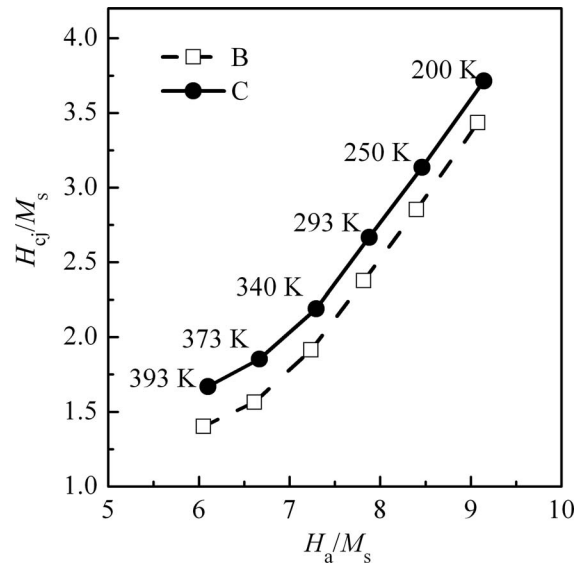


FIG. 10. H_{cj}/M_s varies with H_a/M_s for the optimized magnet (Specimen B) and the GBD treated magnet (Specimen C) at different temperatures.

that the optimized magnet and the GBD treated magnet have almost the same values of intrinsic magnetic properties. In other words, the GBD treatment has little effect on the intrinsic magnetic properties of the main phase of the magnets. Therefore the intrinsic coercivity is enhanced by GBD treatment while the remanence and the maximum energy product almost keep unchanged, which is one of the outstanding advantages of our GBD technique. If the same amount of H_{cj} enhancement is expected, the conventional process may need more Dy to replace Nd. The reduction in B_r is estimated to be 0.8 ~ 1.0 kGs^{40,41} rather than 0.1 to 0.2 kGs.

The intrinsic coercivity may be expressed by the following model:⁴²⁻⁴⁴

$$H_{cj} = \alpha H_a - N_{eff} M_s \quad (1)$$

The first term on the right-hand side reflects the contribution of the magnetocrystalline anisotropy field H_a associated with the microstructure effect represented by parameter α . The second term ' $N_{eff} M_s$ ' is an effective magnetostatic interaction, where N_{eff} is effective demagnetization parameter which mainly depends on the shape and size of the grains of main phase. Here the parameters α and N_{eff} are purely phenomenological and are usually determined by plotting H_{cj}/M_s versus H_a/M_s at different temperatures.

H_{cj}/M_s varies with H_a/M_s at different temperatures is plotted in Fig. 10, which is similar to the H_{cj}/M_s - H_a/M_s plotting on Pr-Fe-B magnet by Sagawa *et al.*⁴³ It can be seen that H_{cj}/M_s has a linear relationship with H_a/M_s for both the optimized magnet and the GBD treated magnet below 340 K. By linear fitting the data between 200 K and 340 K, we obtain (in unit of kOe):

$$H_{cj}(B)/M_s(B) = \alpha(B)H_a(B)/M_s(B) - N_{eff}(B) = 0.825H_a(B)/M_s(B) - 4.07 \quad (2)$$

for the optimized magnet, and

$$H_{cj}(C)/M_s(C) = \alpha(C)H_a(C)/M_s(C) - N_{eff}(C) = 0.823H_a(C)/M_s(C) - 3.81 \quad (3)$$

for the GBD treated magnet. Our α values are about 2.3 times larger than 0.36 on the Pr-Fe-B magnet achieved by Sagawa *et al.*,⁴³ which indicate that the microstructures in our magnets are very much improved to transfer H_a to H_{cj} .

The $H_{cj}(C)$ of the GBD treated magnet as a function of the $H_{cj}(B)$ of the optimized magnet at different temperatures is shown in Fig. 11. It can be seen that the $H_{cj}(C)$ has a very good linear relationship with the $H_{cj}(B)$ within the whole temperature range of measurement. By linear fitting

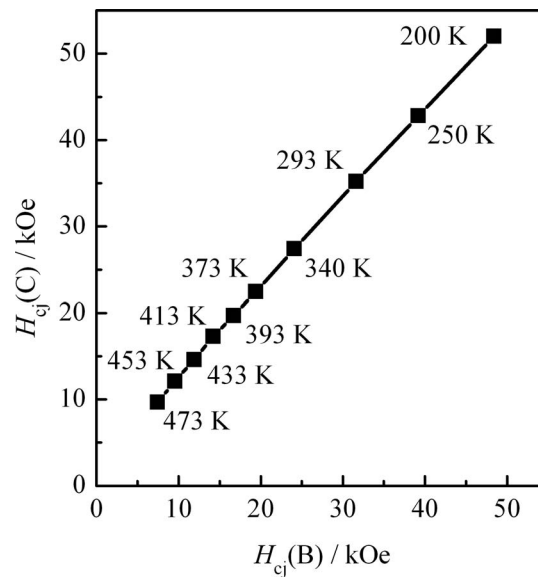


FIG. 11. The intrinsic coercivity of the GBD treated magnet $H_{cj}(C)$ versus the intrinsic coercivity of the optimized magnet $H_{cj}(B)$ at different temperatures.

the data, we obtain (in unit of kOe):

$$H_{cj}(C) = 1.03H_{cj}(B) + 2.38 \quad (4)$$

By bringing equations (2) into equation (4) and taking $M_s(B) \approx M_s(C)$ into consideration, we have (in unit of kOe):

$$H_{cj}(C)/M_s(C) = 0.850[H_a(B) + 2.80]/M_s(C) - 4.20 \quad (5)$$

Equation (5) is slightly different from equation (3).

It has been observed that the modification of coercivity on Nd-Fe-B magnet by the GBD process is sensitive to rare-earth oxides with different rare earths.²² The Tb oxide is the best to increase the H_{cj} due to $Tb_2Fe_{14}B$ with the highest uniaxial anisotropy, while the Sm oxide drastically decreases the coercivity due to $Sm_2Fe_{14}B$ with strong planar anisotropy. This indicates that although the magnetocrystalline anisotropy field H_a keeps unchanged on the entire $Nd_2Fe_{14}B$ -structure main phase during the GBD process, but the H_a of the surface layers of the main phase grains is influenced. By the GBD treatment, the enhancement of intrinsic coercivity H_{cj} is caused not only by the improvement of microstructure but also by the increase of H_a in the grain surface layer. Suppose each main phase grain in sintered magnet is composed of kernel and surface layer. The kernel and surface layer have different intrinsic magnetic properties, especially the magnetocrystalline anisotropic fields. And the GDB treatment only affects the properties of surface layer. Then we may write the following relationship for $H_{cj}(C)$ (assuming $M_s(B) \approx M_s(C)$):

$$H_{cj}(C)/M_s(C) = [\alpha(B) + \Delta\alpha][H_a(B) + \Delta H_a]/M_s(C) - [N_{eff}(B) + \Delta N_{eff}] \quad (6)$$

Re-writing equation (5) in the form of equation (6) and taking the coefficients of $\alpha(B)$ and $N_{eff}(B)$ from equation (2), one can get $\Delta\alpha = 0.025$, $\Delta H_a = 2.80$ kOe, and $\Delta N_{eff} = 0.13$. The H_{cj} enhancement seems to be from two parts respectively: the microstructure improvement by 3% ($\Delta\alpha/\alpha(B)$) and the H_a increase of the surface layers of the main phase grains by 2.80 kOe. And the H_{cj} is weakened by the magnetostatic interaction increase by 3% ($\Delta N_{eff}/N_{eff}(B)$).

Improving H_{cj} is an important way to increase thermal stability of magnets.⁶ Contradicting to the large magnetocrystalline anisotropy field H_a of $Nd_2Fe_{14}B$ -type main phase, the intrinsic coercivity H_{cj} of sintered magnet is far lower than H_a . For example, at room temperature the H_a is 76 kOe for $Nd_2Fe_{14}B$ compound. But for sintered Nd-Fe-B magnet without heavy rare earth, the corresponding intrinsic coercivity H_{cj} is only 11 kOe for conventional manufacture routine. The ratio of H_{cj} to H_a

TABLE III. Weight loss of PCT (120 °C, 100%RH relative humidity, with condensation of water vapor).

Weight loss Exposing time	Whole surface (mg/cm ²)		Two pole surface (mg/cm ²)	
	96 h	96 h + 96 h	96 h	96 h + 96 h
Specimen B	-1.3	-3.2	-2.5	-6.2
Specimen C	-1.4	-2.7	-2.7	-5.2

is $H_{cj}/H_a = 14.5\%$. Many activities have been focusing on narrowing this gap and increase the ratio. By reducing the jet milling particle size to $1\mu\text{m}$, the H_{cj} can reach 20 kOe and $H_{cj}/H_a = 26\%$.⁴ In this work, at temperature of 20 °C, the $H_{cj}/H_a = 31.6\text{kOe}/104\text{kOe} = 30.4\%$ for the optimized magnet and $H_{cj}/H_a = 35.2\text{kOe}/104\text{kOe} = 33.8\%$ for GBD treated magnet. The advantage of our GBD process is to enhance the intrinsic coercivity about 11.4%, but only to reduce the remanence about 1.5%.

D. Corrosion resistance before and after GBD treatment

The corrosion resistance of magnets has been examined by Pressure Cooker Test (PCT) for 96 hours and 192 hours under the condition of 120 °C, 100%RH relative humidity, with condensation of water vapor (according to JEDEC standard: JESD22-A102D, Accelerated Moisture Resistance-Unbiased Autoclave). The weight loss of a sintered magnet is defined by $WL = (W_1 - W_0)/S_0$ in which W_0 and W_1 are the weight of the sample before and after test, and S_0 is the surface area of the sample before test. It was found that both magnets with and without GBD treatment have little difference on weight loss (see Table III). It was also found that the weight loss on the two pole surfaces (c-axis as the normal direction) is much bigger than that of the side surfaces (in which the c-axis lies). This anisotropic corrosion phenomena was also observed by others.^{45,46} So, the weight losses of unit surface area from PCT were calculated in two ways: weight loss divided either by total surface area or only by area of two pole surfaces. The absolute value of weight losses for both samples are $\leq 3.2\text{ mg/cm}^2$ based on the total surface, and $\leq 6.2\text{ mg/cm}^2$ based on the two pole surface. The latter is almost doubled. The PCT result indicates that our GBD treatment has no negative effect on the corrosion resistance of the magnets.

IV. CONCLUSION

In this work, we have developed a new procedure to significantly improve H_{cj} and keep a high maximum energy product of sintered Nd-Fe-B magnet. This new procedure is an optimized routine compare to the conventional one. It consists of an optimized composition design, optimized strip casting, jet milling and low temperature sintering, especially an excellent grain boundary diffusion (GBD) technique.

A magnet with remarkably high performance has been achieved with intrinsic coercivity H_{cj} as 35.2 kOe (2803 kA/m) and maximum energy product $(BH)_{\text{max}}$ as 40.4MGOe (321.6kJ/m^3) at 20 °C. They give H_{cj} (kOe) + $(BH)_{\text{max}}$ (MGOe) > 75. The temperature coefficients of remanence and intrinsic coercivity between temperature of 20 °C and 200 °C are $\alpha_{Br}(C) = -0.122\text{ \%/}^\circ\text{C}$ and $\alpha_{Hcj}(C) = -0.403\text{ \%/}^\circ\text{C}$, respectively. A maximum operating temperature of 230 °C is obtained with permeance coefficient $P_c = -B/H = 2$. It is found that the intrinsic coercivity of the GBD treated magnet $H_{cj}(C)$ has a linear relationship with that of non-treated magnet $H_{cj}(B)$ between 200 K and 393 K: $H_{cj}(C) = 1.03H_{cj}(B) + 2.38$. The enhancement of H_{cj} by GBD treatment has contributions not only from the improvement of microstructure but also from the increase of H_a in the grain surface layer.

Taking the measurement uncertainty into consideration, the intrinsic properties of $4\pi M_s$, H_a and T_C values of the GBD treated magnet are nearly the same as the optimized magnet without GBD treatment. It indicates that our new GBD process has no obvious effect on the Nd₂Fe₁₄B-structure main phase in the magnets. The Dy diffusion mainly affects the microstructure of the optimized

magnet and increase the magnetocrystalline anisotropic field in surface layer of main phase grain to enhance the intrinsic coercivity H_{cj} without significant reduction of the remanence B_r and the maximum energy product $(BH)_{max}$. Our new GBD method also brings no deterioration in corrosion resistance of magnet.

ACKNOWLEDGMENTS

This work was supported by the National High-Tech Research and Development Program of China (863 Program). The project numbers are 2010AA03A401 and 2011AA03A401.

- ¹ M. Sagawa, S. Fujimura, N. Togawa, H. Yamamoto, and Y. Matsuura, *J. Appl. Phys.* **55**, 2083 (1984).
- ² J. J. Croat, J. F. Herbst, R. W. Lee, and F. E. Pinkerton, *J. Appl. Phys.* **55**, 2078 (1984).
- ³ A. S. Kim and F. E. Camp, *J. Appl. Phys.* **79**, 5035 (1996).
- ⁴ R. Goto, M. Matsuura, S. Sugimoto, N. Tezuka, Y. Une, and M. Sagawa, *J. Appl. Phys.* **111**, 07A739 (2012).
- ⁵ H. Sepehri-Amin, Y. Une, T. Ohkubo, K. Hono, and M. Sagawa, *Scripta Mater.* **65**, 396 (2011).
- ⁶ B. M. Ma, W. L. Liu, Y. L. Liang, D. W. Scott, and C. O. Bounds, *J. Appl. Phys.* **75**, 6628 (1994).
- ⁷ S. Pandian, V. Chandrasekaran, G. Markandeyulu, K. J. L. Iyer, and K. Rao, *J. Alloys Compd.* **364**, 295 (2004).
- ⁸ R. S. Mottram, A. J. Williams, and I. R. Harris, *J. Magn. Magn. Mater.* **217**, 27 (2000).
- ⁹ M. Sagawa, S. Fujimura, H. Yamamoto, Y. Matsuura, and K. Hiraga, *IEEE Trans. Magn.* **20**, 1584 (1984).
- ¹⁰ J. F. Herbst, *Rev. Mod. Phys.* **63**, 819 (1991).
- ¹¹ L. Pareti, F. Bolzoni, M. Solzi, and K. H. J. Buschow, *J. Less-Common Met.* **132**, L5 (1987).
- ¹² P. C. Dent, *J. Appl. Phys.* **111**, 07A721 (2012).
- ¹³ M. Endoh, M. Tokunaga, and H. Harada, *IEEE Trans. Magn.* **23**, 2290 (1987).
- ¹⁴ J. Strzeszewski, G. C. Hadjipanayis, and A. S. Kim, *J. Appl. Phys.* **64**, 5568 (1988).
- ¹⁵ S. Hirosawa, H. Tomizawa, S. Mino, and A. Hamamura, *IEEE Trans. Magn.* **26**, 1960 (1990).
- ¹⁶ W. Rodewald and W. Fernengel, *IEEE Trans. Magn.* **24**, 1638 (1988).
- ¹⁷ S. Pandian, V. Chandrasekaran, G. Markandeyulu, K. J. L. Iyer, and K. Rao, *J. Appl. Phys.* **92**, 6082 (2002).
- ¹⁸ M. Tokunaga, H. Kogure, M. Endoh, and H. Harada, *IEEE Trans. Magn.* **23**, 2287 (1987).
- ¹⁹ G. H. Yan, R. J. Chen, Y. Ding, S. Guo, D. Lee, and A. R. Yan, in *2nd International Symposium on Advanced Magnetic Materials and Applications, Sendai, 2010*, edited by M. Takahashi, H. Saito, S. Yoshimura, K. Takanashi, M. Sahashi, and M. Tsunoda [J. Phys.: Conference Series **266** No.012052 (2011)].
- ²⁰ H. Nakamura, K. Hirota, T. Minowa, and M. Honshima, in *IEEE International Magnetism Conference, Nagoya, 2005* [*IEEE Trans. Magn.* **41**, 3844–3846 (2005)].
- ²¹ K. Hirota, H. Nakamura, T. Minowa, and M. Honshima, *IEEE Trans. Magn.* **42**, 2909 (2006).
- ²² H. Nakamura, K. Hirota, T. Minowa, and M. Honshima, *J. Magn. Soc. Jpn.* **31**, 6 (2007).
- ²³ D. Li, S. Suzuki, T. Kawasaki, and K. Machida, *Jpn. J. Appl. Phys.* **47**, 7876 (2008).
- ²⁴ N. Oono, M. Sagawa, R. Kasada, H. Matsui, and A. Kimura, *J. Magn. Magn. Mater.* **323**, 297–300 (2010).
- ²⁵ N. Watanabe, M. Itakura, N. Kuwano, D. Li, S. Suzuki, and K. Machida, *Mater. Trans.* **48**, 915 (2007).
- ²⁶ H. Nakamura, K. Hirota, T. Ohashi, and T. Minowa, *J. Phys. D: Appl. Phys.* **44**, 064003 (2011).
- ²⁷ M. S. Yasuhiro Une, *J. Jpn. Inst. Met.* **76**, 12 (2012).
- ²⁸ B. C. Chen, X. M. Liu, R. J. Chen, S. Guo, D. Lee, and A. Yan, *J. Alloys Compd.* **516**, 73 (2012).
- ²⁹ J. Fidler and T. Schrefl, *J. Appl. Phys.* **79**, 5029 (1996).
- ³⁰ M. Katter, L. Zapf, R. Blank, W. Fernengel, and W. Rodewald, *IEEE Trans. Magn.* **37**, 2474 (2001).
- ³¹ Y. Kato, *J. Appl. Phys.* **85**, 4868 (1999).
- ³² G. Bai, R. W. Gao, Y. Sun, G. B. Han, and B. Wang, *J. Magn. Magn. Mater.* **308**, 20 (2007).
- ³³ R. Kopp, F. Hagemann, L. Hentschel, J. W. Schmitz, and D. Senk, *J. Mater. Process. Technol.* **80-1**, 458 (1998).
- ³⁴ B. Wang, H. Q. Liu, R. W. Gao, and G. B. Han, *J. Funct. Mater. Devices* **10**, 37 (2004).
- ³⁵ A. S. Kim and F. E. Camp, *IEEE Trans. Magn.* **31**, 3656 (1995).
- ³⁶ Y. Matsuura, S. Hirosawa, H. Yamamoto, S. Fujimura, and M. Sagawa, *Appl. Phys. Lett.* **46**, 308 (1985).
- ³⁷ D. X. Chen, E. Pardo, and A. Sanchez, *IEEE Trans. Magn.* **38**, 1742 (2002).
- ³⁸ C. D. Fuerst, J. F. Herbst, and E. A. Alson, *J. Magn. Magn. Mater.* **54-7**, 567 (1986).
- ³⁹ R. Grössinger, R. Krewenka, X. K. Sun, R. Eibler, H. R. Kirchmayr, and K. H. J. Buschow, *J. Less-Common Met.* **124**, 165 (1986).
- ⁴⁰ L. Q. Yu, Y. H. Wen, and M. Yan, *J. Magn. Magn. Mater.* **283**, 353 (2004).
- ⁴¹ P. Tenaud, F. Vial, and M. Sagawa, *IEEE Trans. Magn.* **26**, 1930 (1990).
- ⁴² F. Kools, *J. Phys.* **46**, C6-349 (1985).
- ⁴³ M. Sagawa and S. Hirosawa, *J. Phys.* **49**, C8-617 (1988).
- ⁴⁴ H. Kronmüller, *Phys. Status Solidi B: Basic Research* **144**, 385 (1987).
- ⁴⁵ A. S. Kim, F. E. Camp, and T. Lizzi, *J. Appl. Phys.* **79**, 4840 (1996).
- ⁴⁶ M. Rada, A. Gebert, I. Mazilu, K. Khlopkov, O. Gutfleisch, L. Schultz, and W. Rodewald, *J. Alloys Compd.* **415**, 111 (2006).